Long-term mesospheric record of EPP-IE NO measured by Odin/SMR

Journal of Atmospheric and Solar–Terrestrial Physics 242 (2023) 105997

Contents lists available at ScienceDirect

Journal of Atmospheric and Solar–Terrestrial Physics

journal homepage: www.elsevier.com/locate/jastp

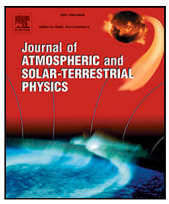

Research paper

Long-term mesospheric record of EPP-IE NO measured by Odin/SMR

Francesco Grieco *, Kristell Pérot, Donal Murtagh

Department of Space, Earth and Environment, Chalmers University of Technology, Gothenburg, Sweden

ARTICLE INFO

Keywords:
Nitric oxide (NO)
Mesosphere
Energetic Particle Precipitation Indirect Effect (EPP-IE)
Odin/SMR

ABSTRACT

Due to the long lifetime of nitric oxide (NO) in darkness conditions, during polar winter, the NO produced by energetic particle precipitation (EPP) in the mesosphere and lower thermosphere (MLT) can descend, via the middle atmospheric residual circulation, to the lower mesosphere and stratosphere, where it is involved in catalytic destruction of ozone (O_3). This process is known as energetic particle precipitation indirect effect (EPP-IE). There are still significant uncertainties on the estimated amount of EPP-IE NO. To improve such estimations, we measure the total winter flux of EPP-IE NO descending through three isentropic levels in the mesosphere, that is 2600 K, 3300 K and 4000 K, based on 15 years of NO nighttime observations from the Sub-Millimetre Radiometer (SMR) on board Odin satellite. At the moment, Odin/SMR is the only instrument ensuring a global coverage of mesospheric NO observations within a few days and this is the first time EPP-IE NO has been quantified using its NO data set. Moreover, such an estimate had never been calculated for the most recent winters which are included in this study. In our method we calculate the median nighttime NO inside the polar vortex during the month prior to the descent of NO-rich air; this value is assumed as a background, produced by N_2O oxidation, to be subtracted from the daily median nighttime concentrations inside the vortex; the result of this subtraction is then multiplied by the area of the vortex and the descent rate to obtain the flux; finally these daily quantities and integrated to calculate the total NO flux for each winter. We thus calculated the total EPP-IE NO flux through the mentioned levels for Northern Hemisphere (NH) winters between 2006–07 and 2020–21 and for Southern Hemisphere (SH) winters between 2007 and 2012. The total winter EPP-IE NO fluxes presented in this study are consistent with the quantities presented in similar studies. NH winters 2008–09, 2012–13 and 2018–19 are the ones presenting the highest NO fluxes at all levels. They are winters characterised by sudden stratospheric warmings followed by elevated stratopause (SSW-ES) events. The measured fluxes vary between 490 and 1000 Mmol at 4000 K, 310 and 720 Mmol at 3300 K, 270 and 510 Mmol at 2600 K. All other NH and SH winters are characterised by sensibly lower values than SSW-ES winters. The fluxes from these more dynamically quiet winters vary from winter to winter following a trend similar to the one of geomagnetic activity, as indicated by the variations in Ap index. These results indicate that the variability in the total EPP-IE NO fluxes is dominated by dynamics during the SSW-ES winters, whereas during the remaining winters it is geomagnetic activity that plays a major role.

1. Introduction

Nitric oxides (NO_x) are involved in the ozone (O_3) catalytic destruction which causes O_3 depletion in the upper stratosphere (Crutzen, 1970). Among these species, in the stratosphere, NO is mainly produced from oxidation of N_2O coming from the troposphere (e.g., McElroy and McConnell, 1971), whereas energetic particle precipitation (EPP) becomes the dominant source towards higher altitudes (Sinnhuber et al., 2012). EPP refers to the process by which protons and electrons, mainly originating either directly from the Sun or from the Earth's radiation belts, interact with the atmosphere.

Solar proton events (SPE) occur when protons originating from solar coronal mass ejections reach energies of tens to hundreds of MeV. During these episodes, protons can penetrate down to the Earth's stratosphere where they lead to the formation of NO, via dissociation of N_2 and subsequent reaction of atomic nitrogen with O_2 (Crutzen et al., 1975). Observed changes in NO abundance due to SPEs are nowadays well understood (e.g., Jackman et al., 2005, 2014). They occur sporadically and their effect is reasonably well reproduced by atmospheric models (Funke et al., 2011). In the stratosphere and lower mesosphere, EPP production of NO is mainly caused by SPEs, but can also be caused by the precipitation of electrons which are energetic enough to reach mesospheric altitudes (medium energy electrons) (Sinnhuber et al., 2016; Newnham et al., 2018). Such a local production by energetic

* Corresponding author.
E-mail address: francesco.grieco@chalmers.se (F. Grieco).

https://doi.org/10.1016/j.jastp.2022.105997
Received 11 July 2022; Received in revised form 22 November 2022; Accepted 11 December 2022
Available online 19 December 2022

particle precipitation is referred to as EPP direct effect (EPP-DE). In the upper mesosphere and lower thermosphere (MLT), during night-time, NO is solely produced by routine precipitation of low-energy (auroral) electrons and protons, i.e. having energies lower than 30 keV and 1 MeV respectively. During day-time, it is also produced by photodissociation of molecular nitrogen (Mironova et al., 2015). NO concentration increases with height to reach a maximum around 110 km (Siskind et al., 1998). In the sunlit mesosphere, NO is rapidly photodissociated and has a lifetime of less than one day whereas, during polar night conditions, its lifetime can extend to several weeks (Brasseur and Solomon, 2005). Therefore, during polar winter, NO-rich air can be transported down to the lower mesosphere and stratosphere via the downward branch of the middle atmospheric residual circulation, where it can contribute to catalytic ozone destruction. This subsidence of NO produced at higher altitudes is called EPP indirect effect (EPP-IE). Randall et al. (2007) have shown that interannual variability of EPP-IE NO in the Southern Hemisphere (SH) is mainly explained by changes in the level of geomagnetic activity and has little dependence on dynamics (Randall et al., 2007). However, in the northern hemisphere (NH), where dynamical variability is significantly higher, several studies have shown that dynamics played a major role on the EPP indirect effect. In particular, strong NO descents are observed in correspondence of Sudden Stratospheric Warming (SSW) events characterised by an elevated stratopause (ES) (e.g. Pérot and Orsolini, 2021, and references therein). During SSW-ES winters, the polar vortex is disturbed by planetary waves (e.g. Charlton and Polvani, 2007) and, in a second time, the stratopause reforms 10 to 20 km higher than usually. As a consequence, the descent restarts at higher rates and from higher altitudes than during other winters (e.g., Grieco et al., 2021). These conditions are favourable for a more efficient downward transport of NO rich air. In the Northern hemisphere, the role of dynamics variability is predominant compared to that of variability in geomagnetic activity. Large increases in EPP-IE NO concentrations have indeed been observed even during NH winters characterised by low geomagnetic activity (e.g., Siskind et al., 2007; Randall et al., 2009). It has been observed that all reactive nitrogen species (NO_y) which are present in the stratosphere due to EPP are responsible for an average depletion of 10%–15% of stratospheric O_3 (Fytterer et al., 2015). However, while middle atmosphere NO concentration from EPP-DE is today well understood, EPP-IE NO is still underestimated in climate models (Funke et al., 2017). For this reason, long-term satellite observations are needed to determine the contribution of EPP-IE to stratospheric O_3 depletion and, more in general, the effect of solar and geomagnetic activity on the climate system throughout the years.

By measuring middle atmospheric NO since October 2003, the Sub-Millimetre Radiometer (SMR) on board Odin satellite provides one of the longest NO concentration records at these altitudes. We examine high latitude measurements from the SMR data set and identify how the amount of EPP-IE NO varies in the mesosphere throughout the years and why. We also determine the number of NO molecules that descend daily through the mesosphere during polar winters in both hemispheres. Above 60 km altitude, NO amounts to the totality of NO_x (Brasseur and Solomon, 2005) allowing us to estimate the flux of the total EPP-IE NO_x above that altitude. However, below 60 km, NO reacts with O_3 to form NO_2 which is not measured by SMR, making the estimation of NO_x difficult in the lower mesosphere. In Section 2 we present the instrument, as well as other data sets used in the study; in Section 3 the method used to quantify EPP-IE NO descending through the polar mesosphere is described; in Section 4 we show the obtained results and, finally, draw our conclusions in Section 5.

2. Data sets

2.1. Odin/SMR

Odin/SMR (Sub-Millimetre Radiometer) performs limb sounding of the middle atmosphere since the launch, on 20 February 2001, of the Odin satellite into a 600 km sun-synchronous orbit with an inclination of 97.77° and a 18:00 h ascending node. SMR has four sub-millimetre receivers covering frequencies between 486–504 GHz and 541–581 GHz, as well as a millimetre receiver measuring around 118 GHz. In this way, emissions from O_3, H_2O, CO, NO, ClO, N_2O, HNO_3 and O_2 from rotational transitions can be detected (Frisk et al., 2003). The Odin mission is a Swedish-led project in collaboration with Canada, France and Finland. SMR observation time was equally shared between astronomical and atmospheric observations until 2007, when the astronomical part of the mission was concluded. Thereafter, SMR has been employed only for atmospheric measurements, performed via vertical scanning of the atmospheric limb and covering from the upper troposphere to the lower thermosphere. In this study, NO mesospheric measurements are used. They are performed between 45–50 km and 110–115 km, covering latitudes between −82.5° and 82.5° and characterised by a vertical resolution of 7 km. Time series of NO concentration from SMR are shown in Fig. 1 for north and south polar regions. Early years of observation are not shown here since those data have not been used in this study due to their limited number. In fact, before 2007 NO was measured only one day per month, whereas after that the number of measurement days increased to 4 to 5 per month. The monthly number of NO measurement days can occasionally be significantly higher during dedicated observational campaigns (Pérot and Orsolini, 2021). Moreover, the gaps in the data sets observed in Fig. 1 in the whole vertical range from 2013 correspond to periods when the instrument was put in standby mode in order to save batteries during the eclipse season, whereas the data gaps visible around 80 km correspond to areas where the concentrations are below instrument sensitivity. NO concentrations are retrieved from two thermal emission lines at 551.7 GHz using algorithms based on the Optimal Estimation Method (Eriksson, 2020; Rodgers, 2000). Here we use version 3.0 of SMR level 2 NO data, which results from a recent reprocessing of the measurements and for which no proper validation study has been carried out yet. However, an empirical model based on SMR v3.0 measurements developed by Kiviranta et al. (2018) could be used to simulate MLT NO concentrations which presented a variability in accordance with that observed by independent instruments such as SOFIE (Solar Occultation For Ice Experiment), SCIAMACHY (SCanning Imaging Absorption spectroMeter for Atmospheric CHartographY), ACE-FTS (Atmospheric Chemistry Experiment-Fourier Transform Spectrometer) and MIPAS (Michelson Interferometer for Passive Atmospheric Sounding).

In addition to the NO data set, we used SMR temperature measurements of the polar regions between 45–90 km altitude from the version 3.0 level 2 data sets presented in Grieco et al. (2021). The temperature from these data sets, which is retrieved from the 556.9 GHz H_2O emission line, has been used to calculate the stratopause height – that is the height of the temperature maximum – for the purpose of identifying SSW-ES winters (see Section 1).

SMR also measures the middle atmospheric tracer species CO and H_2O. It has been considered to use these measurements to investigate the linear correlation between these species and NO, and to calculate the descent rate in the polar vortex. However, the coverage of SMR and the number of available coincidences between these observations and NO observations were not sufficient to do so. This explains why we needed to use external data, as described in the next sub-section.

2.2. MERRA-2

To estimate the amount of NO transported down during polar winter by the downward branch of the middle atmospheric residual circulation, we need to determine the edge of the polar vortex and the descent rate inside of it. For that purpose, three dimensional 3-hourly time-averaged wind and potential vorticity data from the Modern-Era Retrospective analysis for Research and Applications version 2 (MERRA-2) (data set name M2T3NVASM.5.12.4) (Global Modeling and Assimilation Office (GMAO), 2015a) have been used to identify the

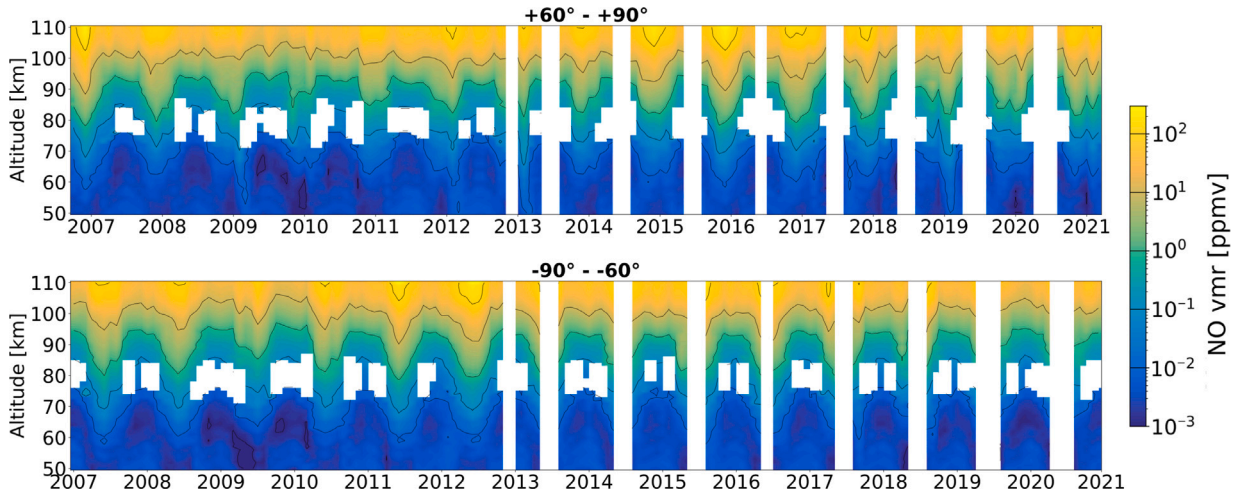

Fig. 1. Time series of monthly medians of NO volume mixing ratios measured by SMR between October 2006 and March 2021 in the +60° – +90° latitude band (top), and between January 2007 and December 2020 in the −90° – −60° latitude band (bottom). The white areas correspond to periods and altitudes at which, in the given latitude band, there are less than 10 measurements. The ticks on the x-axis correspond to the beginning of each year.

edge of the vortex, whereas temperature and heating rate data (data set name M2T3NVRAD.5.12.4) (Global Modeling and Assimilation Office (GMAO), 2015b) have been employed for the calculation of the descent rate. The methods used are presented in Section 3. MERRA-2 is a National Aeronautics and Space Administration (NASA) atmospheric reanalysis (Gelaro et al., 2017) which assimilates various satellite-based data using the Atmospheric Data Assimilation System (ADAS) from the Goddard Earth Observing System Model, Version 5 (GEOS-5). The grid of the data consist of 72 vertical levels between 985–0.01 hPa, covering altitudes from the troposphere to the upper mesosphere, 576 longitude levels 0.625°-wide and 361 latitude levels 0.5°-wide (Bosilovich et al., 2016).

2.3. Ancillary data

In order to identify the periods when the measured NO concentration could potentially be affected by EPP-DE, we have used proton flux data from the NASA Geostationary Operational Environmental Satellites (GOES) to know when SPE events have occurred. These satellites have been carrying on board the Space Environment Monitor (SEM) instrument subsystem which measures, among other variables, proton fluxes originating from the Sun (https://www.ngdc.noaa.gov/stp/satellite/goes/index.html).

We have also been looking at the correlation between variations in geomagnetic activity and EPP-IE NO flux (Section 4). For this purpose, we observe trends in the winter means of Ap index values, as provided by the German Research Centre for Geoscience based in Potsdam, Germany (Matzka et al., 2021a). The Ap index is a daily indicator of the intensity of geomagnetic field disturbances, caused by solar wind and of irregular appearance. It is calculated as the mean of the values measured at 13 different ground observatories (Matzka et al., 2021b).

3. Method for quantification of EPP-IE NO

In this section, we present the method used to quantify the amount of EPP-NO that, during polar winter, gets transported down through the mesosphere via the downward branch of the middle atmospheric residual circulation. To do that, we first re-grid SMR and MERRA-2 data on the same potential temperature levels ranging from 2600 to 4000 K, corresponding to heights in the lower mesosphere. These levels correspond to altitudes between approximately 50 and 75 km. We limit our study to these altitudes since 50 km is the lowest altitude to which the SMR NO data set is available, whereas 75 km is the highest altitude level where the MERRA-2 analysis extends. Potential temperature is used as the vertical coordinate since it is conserved for adiabatic processes. It is therefore a widely used coordinate to study air motion. As mentioned in Section 1, mesospheric NO is quickly photodissociated when exposed to sunlight and has a lifetime of less than a day. We therefore consider only nighttime NO observations in this study, to be able to determine the effect of polar air descent on NO concentration over longer time periods. However, in early spring, some air parcels might be transported to be in the dark at the moment of the measurement although they have been exposed to sunlight a few hours earlier. This is discussed later in the text. With simple trigonometry, we have calculated that an SMR measurement can be considered to be made during nighttime if

$$SZA > 90 + \cos^{-1}\left(\frac{R}{R+h}\right) \cdot \frac{180}{\pi}. \quad (1)$$

SZA is the solar zenith angle of the measurement in degrees, h is the altitude of the tangent point and R is the radius of the Earth. From SMR data, for each isentropic level, we calculate the median nighttime NO concentration inside the polar vortex over a month (October and April for the NH and SH polar winters, respectively), before the wintertime enhancement due to the descent of NO-rich air from higher altitudes. This value is assumed as a background concentration, corresponding to the NO amount already present in the vortex in early winter. In the MLT, nighttime NO has a lifetime of several weeks, as discussed in Section 1. It is therefore reasonable to assume that there is no sensible change in background NO due to photochemical destruction in the vortex before and during the descent, as long as only polar night data is considered. However, there is a change due to dynamics when air subsides in the polar vortex, since the background value varies with altitude. To take this into account, we assume the maximum error as the uncertainty on the background concentration for each level. That is, we assume the uncertainty to be within the following values: the minimum concentration among the medians of each level minus the corresponding standard deviation of the median, and the maximum concentration plus the corresponding standard deviation of the median. The background median values and their maxima are shown in Tables 1 and 2, for NH and SH winters, respectively.

The background is subtracted from each daily nighttime in-vortex median NO concentration. The resulting concentrations are shown in Figs. 2 and 3 for two exemplary NH and SH winters, respectively; that is the 2018–19 NH winter, characterised by a SSW-ES event, and the dynamically quiet 2010 SH winter. The errors on the resulting concentrations are calculated according to statistical error propagation theory (Taylor, 1982). The figures show results for two isentropic

Table 1
Median background NO concentration calculated for considered NH winters and three selected isentropic levels. The numbers in brackets represent the maximum values which include the error.

	2006–07	2007–08	2008–09	2009–10	2010–11	2011–12	2012–13	2013–14
2600 K	40	29	24	11	10	32	38	30
3300 K	15 (49)	13 (34)	19 (30)	4 (19)	4 (24)	17 (36)	27 (43)	18 (35)
4000 K	26	27	20	15	15	24	32	30

	2014–15	2015–16	2016–17	2017–18	2018–19	2019–20	2020–21
2600 K	39	45	43	42	26	33	29
3300 K	26 (42)	23 (51)	33 (47)	20 (48)	17 (31)	19 (60)	13 (45)
4000 K	27	27	37	41	24	52	38

Table 2
Same as Table 1 but for SH winters.

	2007	2008	2009	2010	2011	2012
2600 K	12	14	3	28	12	23
3300 K	15 (57)	11 (22)	6 (32)	7 (37)	8 (23)	25 (47)
4000 K	40	17	23	14	17	38

surfaces, 3300 K and 4000 K, corresponding to heights in the lower and mid-mesosphere, respectively. It should be noted that the winter 2018–2019 was affected by a data gap between mid-November and mid-December, due to instrumental problems. Given the above observations about background NO, with this method we are assuming that any increase in NO concentration inside the vortex is due to EPP-IE. The limitations of this assumption are discussed below.

The method that has been described is similar to the subtraction method presented in Holt et al. (2012). In their study, the method was applied to NO_2 concentration and was validated against a tracer correlation method. We have chosen this method instead of a tracer correlation one because the linear correlation between NO and other spatially and temporally coincident SMR measurements of mesospheric tracers, such as CO and H_2O, was not clear, based on the insufficient available coincidences.

The location of the polar vortex edge is calculated, for each isentropic level and longitude bin, based on MERRA-2 wind and potential vorticity data using a method similar to the one presented by Nash et al. (1996). The edge is located at the latitude where the potential vorticity gradient is maximum, with the constraint that there is a relative maximum wind value within 2°. Moreover, an uncertainty of 2° has been assumed on the latitude of the vortex edge – corresponding to an error on the area between ~2 and ~ $4\ 10^6$ km^2 – as this is approximately the size of the boundary region found by Nash et al. (1996). This method has been chosen in spite of others relying on the gradient of tracer concentrations (e.g. Harvey et al., 2015, 2018), due to the insufficient temporal and spacial sampling of the coincident SMR tracer measurements. The downside is that this introduces further uncertainty because the reanalyses are not constrained by observations in the considered altitude range (Harvey et al., 2015).

Finally, to calculate the daily EPP-IE NO flux (Figs. 2d and 3d) descending through the mesosphere, the daily in-vortex median concentrations resulting from the subtraction method are multiplied by the area enclosed by the vortex (Figs. 2b and 3b). This calculation provides us with the excess number of molecules on each isentropic surface, which was then multiplied by the daily mean descent rate (w) inside the vortex (Figs. 2c and 3c). The latter was calculated from MERRA-2 potential temperature (θ), temperature (T) and heating rate (Q) via the relation (Sagi et al., 2014):

$$w = \frac{\theta}{T} \cdot Q. \quad (2)$$

The obtained descent rates magnitude and winter-time evolution are in accordance with the ones presented in other studies (e.g. Holt et al., 2012). These calculations result in the number of NO molecules crossing each considered isentropic surface, for every measurement day, hereby referred to as EPP-IE NO flux.

The evolution of daily fluxes throughout each winter observed by Odin/SMR, as well as the total value integrated over each winter are expressed in units of megamoles per day and megamoles, respectively. The latter quantity was calculated by summing each daily contribution and by linearly interpolating over the days without SMR observations. The obtained estimates are obviously affected by the irregular temporal sampling of SMR observations, especially in the case of winters affected by a data gap, like the northern winter 2018–2019. They are shown and discussed in Section 4. The errors on both daily fluxes and total winter fluxes are calculated according to statistical error propagation theory (Taylor, 1982).

Our method assumes that NO has not yet been lost by photochemical destruction. Moreover, we include only observations made inside the vortex. These assumptions lead to an underestimate in the calculated NO fluxes. This will be discussed further in the following sections.

Moreover, we use GOES proton flux data to identify the periods when a SPE has occurred and where the observed NO concentration might therefore not only originate from EPP-IE but also significantly be affected by local production at the considered levels. A day is considered to be affected by a SPE if the proton flux is above the Space Weather Prediction Centre threshold of 10 $particles/sr \cdot cm^2 \cdot s$ for protons with energy >10 MeV (https://www.swpc.noaa.gov/products/goes-proton-flux).

4. Results

Comparing Figs. 2 and 3 helps us understand how the flux of nitric oxide descending through the mesosphere during winter-time is affected by dynamics. As previously explained, Fig. 3 corresponds to a standard, dynamically quiet, winter in the Southern hemisphere while Fig. 2 corresponds to a Northern winter affected by a SSW event, with a central date on January 1 (Pérot and Orsolini, 2021), followed by the formation of an elevated stratopause.

Panels 2b and 3b show how the vortex area evolves in different ways during these two winters. In 2010 it is relatively stable around a standard value of about 15 million km^2, whereas in 2018–19 the values observed for one month following the central date, especially at 3300 K, are significantly smaller than the ones registered on the rest of the winter, due to the breakdown of the vortex.

In panels 2c and 3c it can be seen how during a SSW-ES winter higher descent rates are reached compared to a dynamically quiet winter. In NH 2018–19 winter, the descent stops around the SSW central date (with the descent rate reaching positive values), due to the disruption of the polar vortex; then the polar vortex recovers and the descent rates at both considered heights show an abrupt increase in the end of January. It reaches a value of −7 km/day at 4000 K, which is a significantly higher value than the −4 km/day characterising the pre-SSW period and the dynamically quiet SH 2010 winter. Moreover, in Figs. 2a and 3a it can be seen how higher concentrations are measured during NH 2018–19 with respect to SH 2010 (see Section 1). Higher NO concentration and higher descent rates during NH 2018–19, following the SSW-ES event, cause daily NO fluxes across the considered surfaces

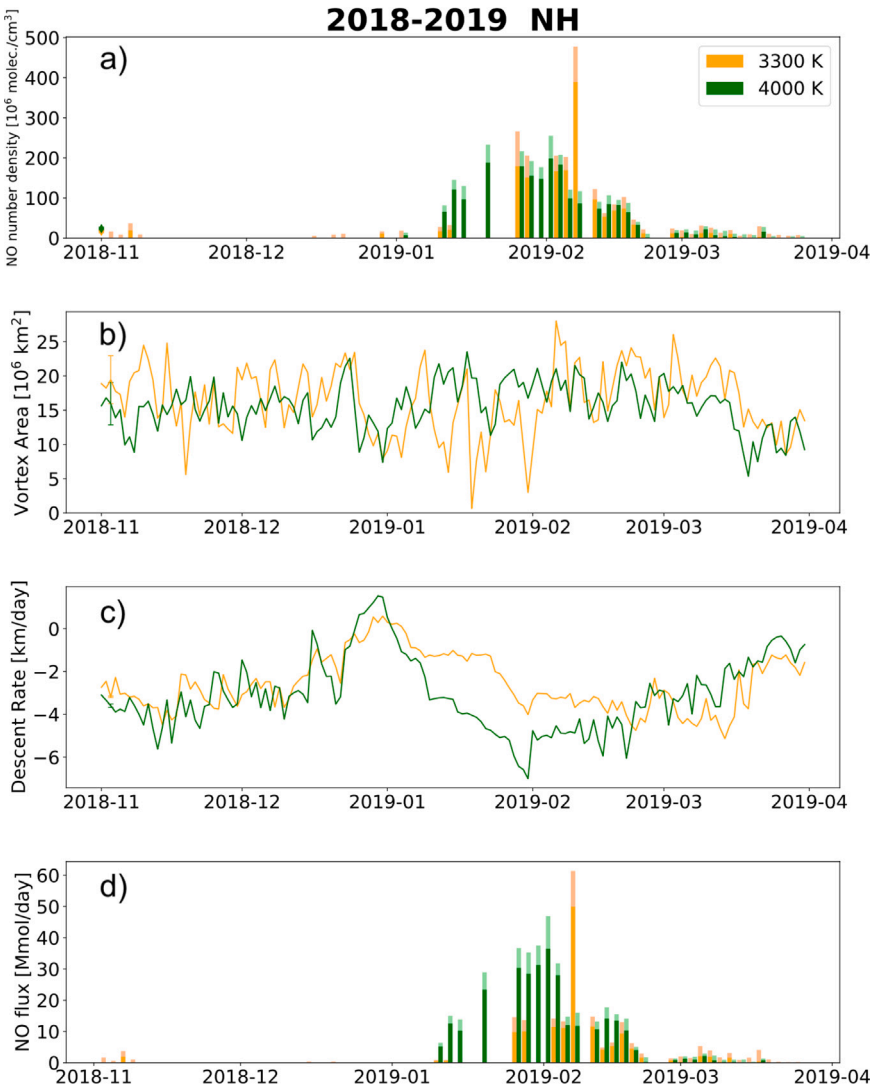

Fig. 2. Daily medians of the quantities used to calculate NO fluxes through two isentropic surfaces, and resulting daily fluxes for one exemplary winter characterised by a SSW-ES event, that is northern winter 2018–19. In particular, NO measured number density (from which the background has been subtracted) is plotted in panel (a), vortex area in panel (b), descent rate in panel (c), NO flux in panel (d). The diamonds in panel (a) represent the subtracted background. The data plotted in panels (a) and (d) correspond to SMR observations days, with darker coloured bars representing the median value and lighter coloured ones representing the median plus 1 σ; whereas (b) and (c) show data obtained from MERRA-2 as explained in the text, for every day, with only one exemplary error bar shown for clarity reasons.

to be up to an order of magnitude higher than during SH 2010, as can be seen in Figs. 2d and 3d.

Figs. 4 and 5 show time series of daily NO flux through the three selected levels for all available NH and SH winters, respectively. This was calculated using the method described in the previous section. Except for the winters which are affected by SPEs, the NO flux is to be attributed to EPP-IE. SPE are represented by the grey bars in Figs. 4 and 5.

Note that the 2600 K level is shown for Figs. 4 and 5 but not for Figs. 2 and 3. This was done to make Figs. 2 and 3 clearer and, most importantly, because at 2600 K NO and NO_x concentrations do not coincide, due to NO reacting with O_3 to form NO_2, as explained in Section 1. SMR does not measure NO_2, making it hard to estimate NO_x at 2600 K.

The histograms in Figs. 6a and 7a show the total flux of EPP-NO that was transported downward through the mesosphere, at three selected isentropic levels in the lower mesosphere, namely 2600, 3300 and 4000 K, during each winter observed by SMR after October 2006. The corresponding values are also reported in Tables 3 and 4. Note that a smaller number of SH winters, compared to NH winters, is considered in this study due to the data gaps that affect SH winters from 2013 onward (see Section 2.1 and Fig. 1).

When interpreting these results, it is important to keep in mind the limitations of our method to estimate the NO fluxes. As mentioned in Section 3, the calculated total winter fluxes are affected by the temporal distribution of SMR measurements. Data gaps, especially the longer ones due to instrumental problems like in November–December 2018, do not allow to account for possible variations in the NO concentration (and therefore fluxes) during given periods. Such long gaps however rarely occurs outside the standby periods to save the battery (see Section 1). In such cases, values from the linear interpolation of the adjacent measurement days are used for the calculation of the total flux, instead. Moreover, the method used in this study (see Section 3) leads to a possible underestimation of the EPP-IE NO flux. This happens because of the assumption that by including only nighttime measurements for the calculation of the median, we are not including parcels of air that have been exposed to sunlight. It might in fact happen that, in early spring, some of the air parcels that were transported to be in the dark at the moment of the measurement have been in a sunlit part of the globe a few hours earlier. In such cases, a part of the descending NO would be photolysed, leading to an underestimation of the EPP-IE

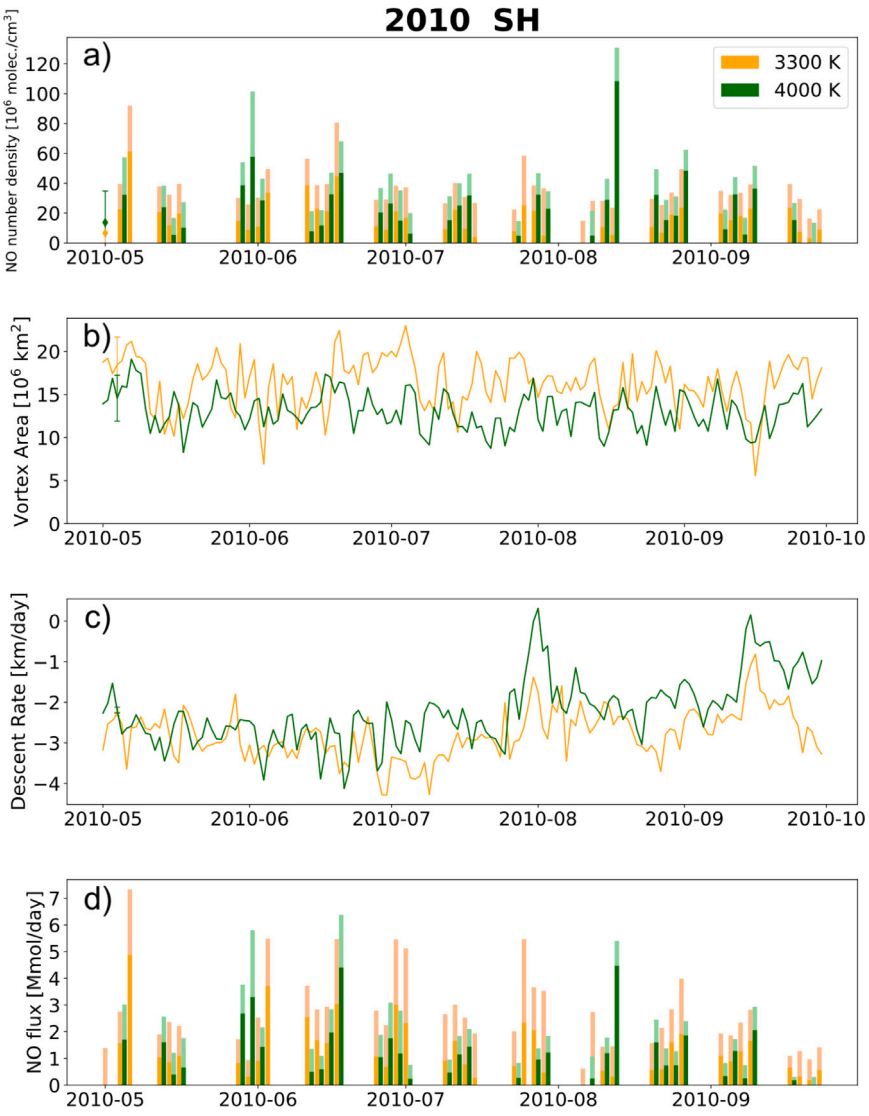

Fig. 3. Same as Fig. 2 but for a dynamically quiet winter, that is southern winter 2010.

NO flux value. For this reason, in the following part of this manuscript, we will discuss values corresponding to the median plus one standard deviation, rather than the median itself, because we believe that these values are more representative of the actual EPP-NO fluxes.

Moreover, to compare our results with levels of geomagnetic activity, time series of winter means of daily Ap index are shown in Figs. 6b and 7b for NH and SH, respectively.

From daily medians of SMR temperature measurements (Grieco et al., 2021) in the polar regions, we calculate the height of the stratopause – that is the height of the temperature maximum – for every day during the period considered in this study. Time series of the stratopause height are shown in Figs. 6c and 7c for the +60° – +90° region and the −90° – −60° region, respectively. This has been done to clearly identify winters which are characterised by an ES. It can be seen how, during the considered period, such events have occurred several times in the northern polar region, but have never occurred in the southern hemisphere.

Among NH winters, the ones being characterised by the highest NO fluxes, at all three isentropic levels, are winters 2008–09, 2012–13 and 2018–19. These are all winters presenting SSW-ES events, characterised by distinct peaks in Fig. 6c.

These winter fluxes have values ranging between 490 and 1000 Mmol at 4000 K, 310 and 720 Mmol at 3300 K, 270 and 510 Mmol at 2600 K (Fig. 6a). These EPP-IE NO amounts significantly above average are mainly due to higher descent rates observed at high altitudes after the recovery of the vortex (as seen in Fig. 2c for example), allowing NO-richer air to be transported down to the lower mesosphere. It is clear how the amount of NO transported down by the recovered polar vortex decreases towards lower levels, with up to half NO flux dispersing from one level to the next. This can be due to possible leakage from the vortex, especially during winters affected by a SSW. In fact, during the period when the vortex is weaker, the air inside the vortex is exposed to more mixing with air outside of it. Moreover, at 2600 K, lower NO amounts could be explained by partial conversion of NO into NO_2 (see Section 1).

Despite this, SSW-ES winters present the three highest fluxes at all levels, even with the mean geomagnetic activity being lower than most other years (Fig. 6a).

NH total winter fluxes from 2006–07, 2007–08, 2009–10, 2010–11, 2013–14, 2014–15, 2016–17, 2017–18, 2019–20 and 2020–21, as well as all the SH winters shown in Fig. 7a (note that SH winters after 2013 are not studied due to the important data gaps during winter time, as explained in Section 2.1), present sensibly lower values than SSW-ES winters. These more dynamically quiet winters present fluxes changing with time at trends which resemble the ones from the Ap index time series. Flux values vary between 84 and 250 Mmol at 4000 K, 140 and

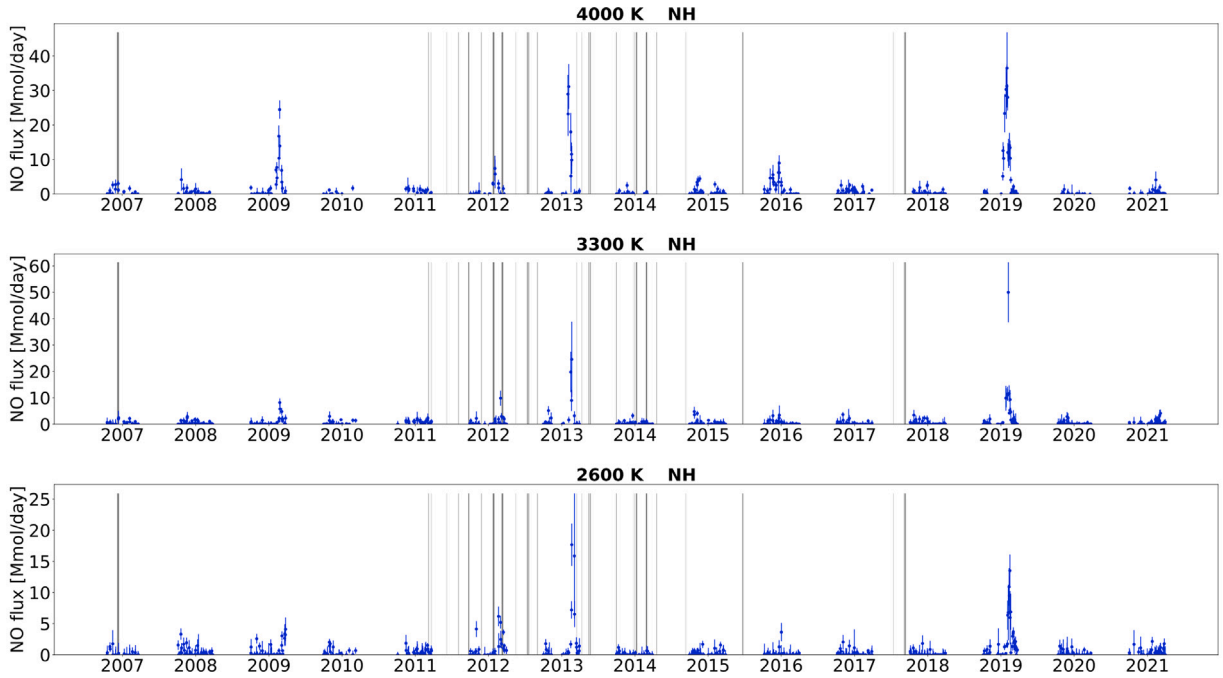

Fig. 4. Time series of NH daily NO flux calculated for considered winters and three selected isentropic levels. Grey bars represent days affected by SPE events. Note the different scales on the y-axis.

Table 3
Total NO flux values shown in Fig. 6a. The values in brackets represent the calculated flux plus 1σ. All values are expressed in Mmol.

	2006–07		2007–08		2008–09		2009–10		2010–11		2011–12		2012–13		2013–14	
2600 K	31	(180)	46	(150)	110	(270)	36	(110)	74	(190)	170	(280)	320	(510)	10	(78)
3300 K	110	(250)	86	(170)	150	(310)	70	(150)	130	(300)	130	(300)	400	(720)	48	(140)
4000 K	150	(250)	61	(140)	350	(490)	59	(130)	120	(240)	190	(350)	630	(860)	21	(84)

	2014–15		2015–16		2016–17		2017–18		2018–19		2019–20		2020–21	
2600 K	32	(130)	14	(120)	24	(110)	18	(110)	240	(380)	15	(110)	63	(180)
3300 K	58	(180)	78	(230)	39	(160)	48	(170)	470	(690)	30	(160)	65	(220)
4000 K	110	(230)	270	(420)	110	(230)	41	(150)	790	(1000)	12	(150)	39	(160)

Table 4
Total NO flux values shown in Fig. 7a. The values in brackets represent the calculated flux plus 1σ. All values are expressed in Mmol.

	2007		2008		2009		2010		2011		2012	
2600 K	120	(290)	82	(240)	74	(200)	51	(200)	120	(270)	62	(190)
3300 K	160	(380)	150	(320)	49	(180)	190	(400)	260	(470)	70	(240)
4000 K	86	(280)	88	(200)	16	(140)	190	(300)	270	(420)	98	(230)

300 Mmol at 3300 K, 78 and 190 Mmol at 2600 K for NH winters. Values up to 420, 470 and 290 Mmol at 4000, 3300 and 2600 K potential temperature levels respectively are reached in SH winters with high geomagnetic activity. These results confirm that the amount of NO that is transported down to the lower mesosphere essentially depends on the production level in the upper mesosphere/lower thermosphere in the Southern hemisphere, while it is strongly dependent on the dynamical activity in the Northern hemisphere. The correlation between EPP-IE NO and geomagnetic activity has already been shown in previous studies such as, e.g., Randall et al. (2007) and Funke et al. (2014). With higher NO concentrations at higher altitudes, it is expected to see highest levels showing the most intense fluxes. In fact, this is actually observed both during SSW-ES winters and most of the dynamically quiet ones. The winters when this is not happening are the ones characterised by descent rates which are greater at lower levels (not shown), resulting in an increase in the observed flux in such levels.

A particular case is NH winter 2011–12 for which higher fluxes can be associated with SPEs (von Clarmann et al., 2013) (as visible in Fig. 4), therefore we will not consider the NO observed being EPP-IE origin in this case. Moreover, in Fig. 6c it is possible to notice how, during this winter, the stratopause is located at a higher altitude than usual, even though not as high as other SSW-ES winters. This suggests the presence of a more modest ES event, which would also help explain the higher fluxes observed. No particularly high NO fluxes have been measured during other years affected by SPE events. Moreover, NH winter 2015–16 shows a flux of medium intensity of 420 Mmol at the 4000 K level due to the occurrence of stronger descents (not shown). To this might also contribute the higher geomagnetic activity recorded during that winter (Fig. 6b).

Funke et al. (2014) use a tracer correlation method based on observations from the Michelson Interferometer for Passive Atmospheric Sounding (MIPAS) to calculate the EPP-NO_y flux (where NO_y includes NO, NO_2, HNO_3, $ClONO_2$ and $2N_2O_5$) for polar winters 2002–2012. They estimate EPP-NO_y flux in different ways, one of which consists of calculating the total hemispheric flux from zonal mean EPP-NO_y densities and descent rates, where descent rates are calculated from MERRA version 1 diabatic heating rates and temperature (Rienecker et al., 2011) similarly to how they are calculated in our study (see

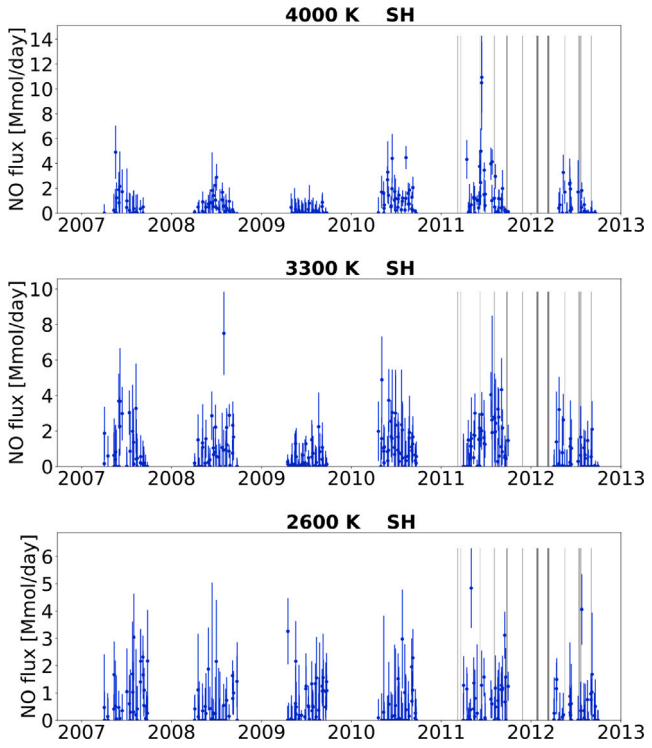

Fig. 5. Same as Fig. 4 but for the Southern hemisphere.

Table 5
SMR EPP-NO fluxes plus 1σ (in black) and MIPAS EPP-NO_y fluxes from Funke et al. (2014) (in brackets, in dark grey) for NH winters.

	2007–08		2008–09		2009–10		2010–11	
2600 K (1 hPa)	150	(370)	270	(250)	110	(140)	190	(230)
3300 K (0.1 hPa)	170	(420)	310	(380)	150	(110)	300	(210)

Table 6
SMR EPP-NO fluxes plus 1σ (in black) and MIPAS EPP-NO_y fluxes from Funke et al. (2014) (in brackets, in dark grey) for SH winters.

	2007		2008		2009		2010		2011	
2600 K (1 hPa)	290	(930)	240	(1200)	200	(580)	200	(860)	270	(1360)
3300 K (0.1 hPa)	380	(770)	320	(820)	180	(310)	400	(670)	470	(1150)

Section 3). This is done for the 1 and 0.1 hPa pressure levels which roughly correspond to the 2600 and 3300 K potential temperature levels considered in our study. Furthermore, there is a temporal overlap between MIPAS and SMR. It is therefore possible to directly compare our fluxes at these two levels with the ones from Funke et al. (2014) (see Tables 5 and 6), although they calculate total hemispheric fluxes whereas we calculate fluxes inside the polar vortex. Moreover, our results are not representative of EPP-NO_y fluxes, due to the presence of NO_y species other than NO at these altitudes (Brasseur and Solomon, 2005), which is particularly true for the 2600 K level where NO reacts with O_3 and forms NO_2, as explained in Section 1. The values presented in Tables 5 and 6 show that for all SH winters and for NH winter 2007–08 our fluxes are considerably lower than the ones measured by Funke et al. (2014), whereas our values for NH winters 2008–09, 2009–10 and 2010–11 are in better agreement with theirs. In general, our estimates seem to be qualitatively consistent in their order of magnitude and inter-annual variability to those by Funke et al. (2014), with similar trends observed in flux values except for NH winter 2008–09 and SH winter 2008.

Another study on EPP-NO_y is the one from Sinnhuber et al. (2018). It focuses on NH and SH winters between 2002 and 2010, and therefore presents temporal overlap with our study. They compare their EPP-NO_y hemispheric maximum concentrations, obtained from three different models, with those obtained by Funke et al. (2014) between 100 and 0.02 hPa, and show good agreement. The inter-annual variability of their results resembles the one from Funke et al. (2014) and ours (except for except NH winter 2008–09 and SH winter 2008). It is however not possible to directly compare our results with theirs since they do not calculate EPP-NO_y fluxes.

Moreover, the values we found are consistent with the ones found by Randall et al. (2007). They focused on SH winters between 1992 and 2005 and measure amounts of EPP-NO_x at 45 km between 0.1 and 2.6 Gmol. As explained in the previous sections, our study is based on NO measurements only and we consider different years than the ones in the above mentioned study. It is therefore not possible to carry out a quantitative comparison between our results and those of Randall et al. (2007). However, given that the winter NO/NO_x ratio above 60 km is approximately 1 (Brasseur and Solomon, 2005), the values we measure at 3300 K and 4000 K can be assumed as to be representative of EPP-NO_x fluxes. They are of the same order of magnitude – although lower – as the ones obtained by Randall et al. (2007).

5. Summary and conclusion

The Sub-Millimetre on board the Odin satellite has been operational for an exceptionally long time and is currently the only instrument observing mesospheric nitric oxide globally. The goal of our study is to quantify the amount of NO transported from the upper mesosphere and lower thermosphere down to the lower mesosphere, based on the unique Odin data set, in order to contribute to a better understanding of the energetic particle precipitation indirect effect.

Starting from 15 years of SMR polar night NO observations in the lower mesosphere, we have subtracted from the daily in-vortex median concentration a background value corresponding to the small amount of NO already present in the vortex in early winter, before the enhancement due to the descent of NO-rich air coming from higher altitudes. We have multiplied the obtained value by the area enclosed by the vortex, and then by the mean descent rate in the vortex. These calculations have resulted in EPP-IE NO fluxes, corresponding to the number of EPP-IE NO molecules crossing the considered isentropic surfaces, namely 2600, 3300 and 4000 K. The amount of NO is a good approximation for the amount of NO_x at the two upper levels, where the NO_2 concentration is negligible. This method has been applied to all SMR night-time observations between 2006 and 2021 in the Northern hemisphere and between 2007 and 2012 in the Southern hemisphere, resulting in time series of daily EPP-IE NO fluxes for all SMR measurement days, as well as estimate of total winter fluxes. We have described the method in details and discussed its limitations.

We found that the highest NH fluxes are observed during winters characterised by SSW followed by an elevated stratopause event (in particular 2008–09, 2012–13, 2018–19), during which the descent of the vortex air is stronger and originating at higher altitudes than usual, where NO concentration is particularly high. In these cases, values vary between 490 and 1000 Mmol at 4000 K, 310 and 720 Mmol at 3300 K, 270 and 510 Mmol at 2600 K. The flux values seem here to be dominated by the middle atmospheric dynamics rather than geomagnetic activity. Exceptions are NH winter 2011–12 (which is affected by SPE) and 2015–16 (characterised by strong descents), all other winters not affected by SSW-ES events present significantly lower NO flux values, and those vary with time following geomagnetic activity trends. In the NH, NO flux values during these dynamically quiet winters are between 84 and 250 Mmol at 4000 K, 140 and 300 Mmol at 3300 K, 78 and 190 Mmol at 2600 K, but reach up to 420, 470 and 290 Mmol at 4000, 3300 and 2600 K levels in the SH. Our results suggest that the EPP-IE NO flux variability is mainly controlled by dynamics during the SSW-ES winters whereas, during the dynamically quiet winters, geomagnetic activity dominates. The order of magnitude of our estimates is consistent with

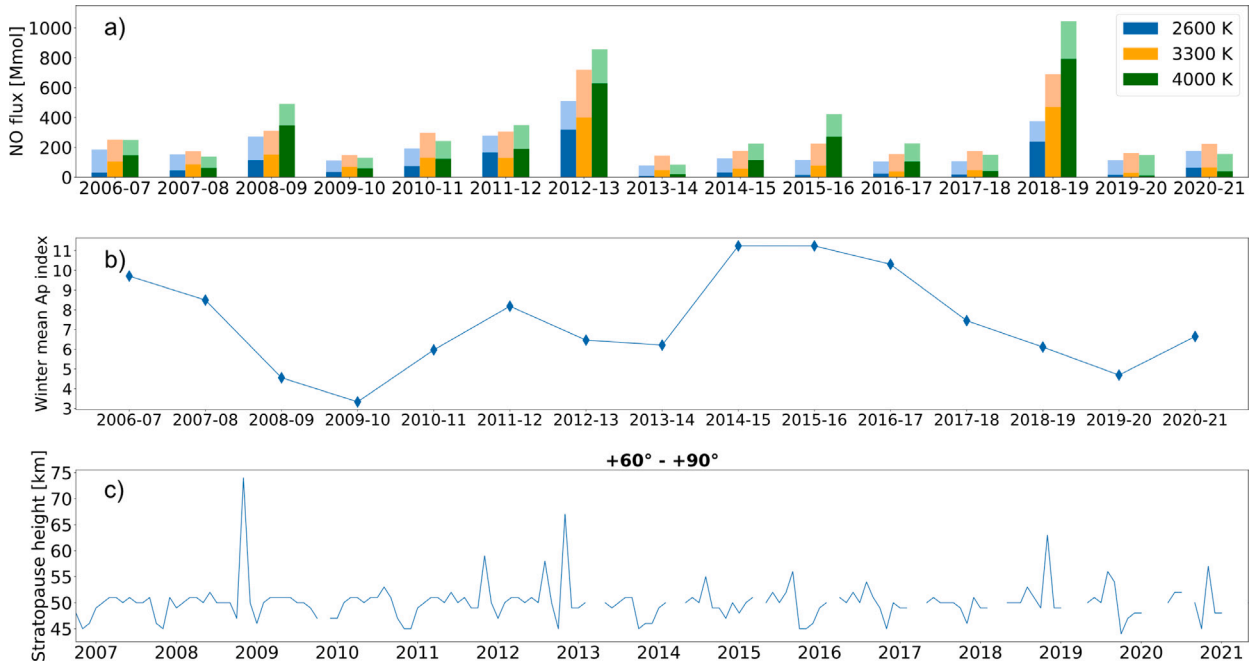

Fig. 6. Panel (a): Total NO flux calculated using the method described in Section 3, across three selected isentropic levels, based on SMR observations, for all Northern winters considered in this study. Darker coloured bars correspond to the median values and lighter coloured bars represent the median plus 1σ. Panel (b): Mean winter Ap index for the same winters. Panel (c): Stratopause height between +60° and +90° latitudes, calculated from daily medians of Odin/SMR temperature measurements. The ticks on the x-axis correspond to the first day of the year.

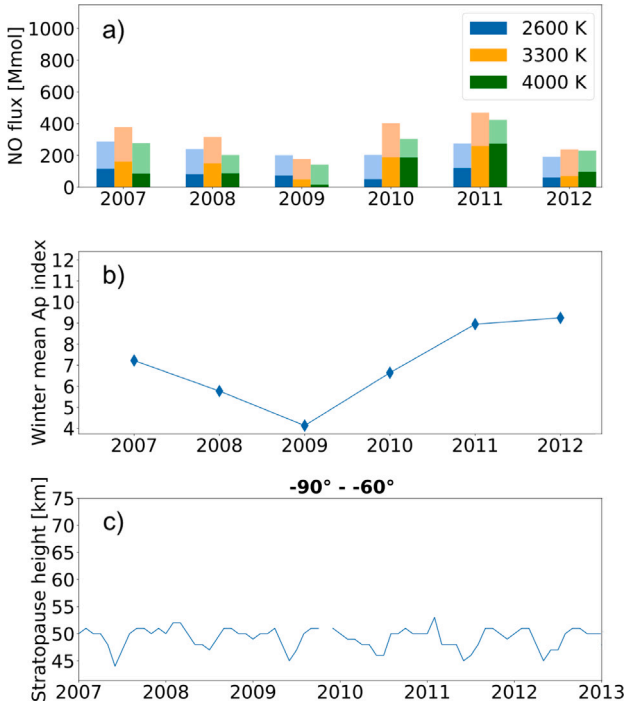

Fig. 7. Same as Fig. 6 but for the Southern hemisphere.

that from Randall et al. (2007) (estimating EPP-NO_x) as well as that from Funke et al. (2014) and Sinnhuber et al. (2018) (both estimating EPP-NO_y), although our values are systematically lower. Causes for the smaller fluxes obtained by us with respect to EPP-NO_y could be that NO is not representative of NO_y at the considered altitudes. Moreover, our smaller flux values with respect to NO_x fluxes at 3300 K and 4000 K – where NO amounts are representative of NO_x amounts – could be due to the underestimation intrinsic to our method, as explained in Section 4. In addition to that, we found that the inter-annual variability of the fluxes reported in our study is qualitatively consistent – except for NH winter 2008–09 and SH winter 2008 – with the variability from Funke et al. (2014) and Sinnhuber et al. (2018), whose data sets present a temporal overlap with SMR.

EPP-IE NO has been quantified for the first time using the unique Odin/SMR NO data set. We presented daily and total winter fluxes for a particularly important number of winters, in both hemispheres, including the most recent winters for which such an estimate had never been calculated, thus extending previous EPP-IE NO time series into the present. Such results can be used to study further the impact of energetic particle precipitation on the atmosphere.

CRediT authorship contribution statement

Francesco Grieco: Made the plots, Wrote most of the text, Interpretation of the results, Discussions. **Kristell Pérot:** Writing of the text, Interpretation of the results, Proofread the text, Discussions, Funding acquisition. **Donal Murtagh:** Discussions, Funding acquisition.

Declaration of competing interest

The authors declare that they have no known competing financial interests or personal relationships that could have appeared to influence the work reported in this paper.

Data availability

Odin/SMR v3.0 L2 data are publicly accessible at http://odin.rss.chalmers.se/level2.

Acknowledgements

Odin is a Swedish-led satellite mission, and is also part of the European Space Agency's (ESA) third party mission programme. The recent reprocessing of the SMR NO data was supported by ESA and by the Swedish National Space Agency (SNSA, Dnr 20/88). The authors acknowledge additional support from SNSA, Sweden (Dnr 184/15). They would also like to thank NASA for making the MERRA-2 and GOES data available, as well as the GFZ German Research Centre for Geosciences for providing the indices of geomagnetic activity. The authors also thank the two anonymous reviewers for carefully reading the manuscript and for their insightful and helpful comments.

References

Bosilovich, M., Lucchesi, R., Suarez, M., 2016. MERRA-2: File specification no. 9 (version 1.1). NASA Global Modeling and Assimilation Office URL https://gmao.gsfc.nasa.gov/pubs/docs/Bosilovich785.pdf.

Brasseur, G., Solomon, S., 2005. Aeronomy of the Middle Atmosphere, third ed Springer, the Netherlands.

Charlton, A., Polvani, L., 2007. A new look at stratospheric sudden warmings. Part I: Climatology and modeling benchmarks. J. Climate 20, 449–469. http://dx.doi.org/10.1175/JCLI3996.1.

Crutzen, P.J., 1970. The influence of nitrogen oxides on the atmospheric ozone content. Q. J. R. Meteorol. Soc. 96 (408), 320–325. http://dx.doi.org/10.1002/qj.49709640815, URL arXiv:https://rmets.onlinelibrary.wiley.com/doi/pdf/10.1002/qj.49709640815.

Crutzen, P.J., Isaksen, I.S.A., Reid, G.C., 1975. Solar proton events: Stratospheric sources of nitric oxide. Science 189 (4201), 457–459, URL http://www.jstor.org/stable/1740489.

Eriksson, P., 2020. Algorithm theoretical basis document: Level 2 processing. Technical Report, Chalmers University of Technology, Department of Space, Earth and Environment, URL https://odin.rss.chalmers.se/static/documents/L2_ATBD.pdf.

Frisk, U., Hagström, M., Ala-Laurinaho, J., Andersson, S., Berges, J.-C., Chabaud, J.-P., Dahlgren, M., Emrich, A., Florén, H.-G., Florin, G., Fredrixon, M., Gaier, T., Haas, R., Hirvonen, T., Hjalmarsson, Å., Jakobsson, B., Jukkala, P., Kildal, P.S., Kollberg, E., Lassing, J., Lecacheux, A., Lehikoinen, P., Lehto, A., Mallat, J., Marty, C., Michet, D., Narbonne, J., Nexon, M., Olberg, M., Olofsson, A.O.H., Olofsson, G., Origné, A., Petersson, M., Piironen, P., Pons, R., Pouliquen, D., Ristorcelli, I., Rosolen, C., Rouaix, G., Räisänen, A.V., Serra, G., Sjöberg, F., Stenmark, L., Torchinsky, S., Tuovinen, J., Ullberg, C., Vinterhav, E., Wadefalk, N., Zirath, H., Zimmermann, P., Zimmermann, R., 2003. The odin satellite I. Radiometer design and test. Astron. Astrophys. 402 (3), L27–L34. http://dx.doi.org/10.1051/0004-6361:20030335.

Funke, B., Ball, W., Bender, S., Gardini, A., Harvey, V.L., Lambert, A., López-Puertas, M., Marsh, D.R., Meraner, K., Nieder, H., Päivärinta, S.-M., Pérot, K., Randall, C.E., Reddmann, T., Rozanov, E., Schmidt, H., Seppälä, A., Sinnhuber, M., Sukhodolov, T., Stiller, G.P., Tsvetkova, N.D., Verronen, P.T., Versick, S., von Clarmann, T., Walker, K.A., Yushkov, V., 2017. HEPPA-II model–measurement intercomparison project: EPP indirect effects during the dynamically perturbed NH winter 2008–2009. Atmos. Chem. Phys. 17 (5), 3573–3604. http://dx.doi.org/10.5194/acp-17-3573-2017, URL https://acp.copernicus.org/articles/17/3573/2017/.

Funke, B., Baumgaertner, A., Calisto, M., Egorova, T., Jackman, C.H., Kieser, J., Krivolutsky, A., López-Puertas, M., Marsh, D.R., Reddmann, T., Rozanov, E., Salmi, S.-M., Sinnhuber, M., Stiller, G.P., Verronen, P.T., Versick, S., von Clarmann, T., Vyushkova, T.Y., Wieters, N., Wissing, J.M., 2011. Composition changes after the "halloween" solar proton event: the high energy particle precipitation in the atmosphere (HEPPA) model versus MIPAS data intercomparison study. Atmos. Chem. Phys. 11 (17), 9089–9139. http://dx.doi.org/10.5194/acp-11-9089-2011, URL https://acp.copernicus.org/articles/11/9089/2011/.

Funke, B., López-Puertas, M., Holt, L., Randall, C.E., Stiller, G.P., von Clarmann, T., 2014. Hemispheric distributions and interannual variability of NOy produced by energetic particle precipitation in 2002–2012. J. Geophys. Res.: Atmos. 119 (23), 13,565–13,582. http://dx.doi.org/10.1002/2014JD022423, URL arXiv:https://agupubs.onlinelibrary.wiley.com/doi/pdf/10.1002/2014JD022423.

Fytterer, T., Mlynczak, M.G., Nieder, H., Pérot, K., Sinnhuber, M., Stiller, G., Urban, J., 2015. Energetic particle induced intra-seasonal variability of ozone inside the antarctic polar vortex observed in satellite data. Atmos. Chem. Phys. 15 (6), 3327–3338. http://dx.doi.org/10.5194/acp-15-3327-2015, URL https://acp.copernicus.org/articles/15/3327/2015/.

Gelaro, R., McCarty, W., Suarez, M.J., Todling, R., Molod, A., Takacs, L., Randles, C.A., Darmenov, A., Bosilovich, M.G., Reichle, R., Wargan, K., Coy, L., Cullather, R., Draper, C., Akella, S., Buchard, V., Conaty, A., da Silva, A.M., Gu, W., Kim, G.-K., Koster, R., Lucchesi, R., Merkova, D., Nielsen, J.E., Partyka, G., Pawson, S., Putman, W., Rienecker, M., Schubert, S.D., Sienkiewicz, M., Zhao, B., 2017. The modern-era retrospective analysis for research and applications, version 2 (MERRA-2). J. Clim. 30 (14), 5419–5454. http://dx.doi.org/10.1175/JCLI-D-16-0758.1, URL https://journals.ametsoc.org/view/journals/clim/30/14/jcli-d-16-0758.1.xml.

Global Modeling and Assimilation Office (GMAO), 2015a. MERRA-2 tavg3_3d_asm_Nv: 3d,3-hourly,time-averaged,model-level,assimilation,assimilated meteorological fields V5.12.4. http://dx.doi.org/10.5067/SUOQESM06LPK, Greenbelt, MD, USA, Goddard Earth Sciences Data and Information Services Center (GES DISC), (Accessed November 2021).

Global Modeling and Assimilation Office (GMAO), 2015b. MERRA-2 tavg3_3d_rad_Nv: 3d,3-hourly,time-averaged,model-level,assimilation,radiation diagnostics V5.12.4. http://dx.doi.org/10.5067/7GFQKO1T43RW, Greenbelt, MD, USA, Goddard Earth Sciences Data and Information Services Center (GES DISC), (Accessed November 2021).

Grieco, F., Pérot, K., Murtagh, D., Eriksson, P., Rydberg, B., Kiefer, M., Garcia-Comas, M., Lambert, A., Walker, K.A., 2021. Improvement of odin/SMR water vapour and temperature measurements and validation of the obtained data sets. Atmos. Meas. Tech. 14 (8), 5823–5857. http://dx.doi.org/10.5194/amt-14-5823-2021, URL https://amt.copernicus.org/articles/14/5823/2021/.

Harvey, V.L., Randall, C.E., Collins, R.L., 2015. Chemical definition of the mesospheric polar vortex. J. Geophys. Res.: Atmos. 120 (19), 10,166–10,179. http://dx.doi.org/10.1002/2015JD023488.

Harvey, V.L., Randall, C.E., Goncharenko, L., Becker, E., France, J., 2018. On the upward extension of the polar vortices into the mesosphere. J. Geophys. Res.: Atmos. 123 (17), 9171–9191. http://dx.doi.org/10.1029/2018JD028815.

Holt, L., Randall, C., Harvey, V., Remsberg, E., Stiller, G., Funke, B., Bernath, P., Walker, K., 2012. Atmospheric effects of energetic particle precipitation in the Arctic winter 1978–1979 revisited. J. Geophys. Res. (Atmospheres) 117, http://dx.doi.org/10.1029/2011JD016663, 5315–.

Jackman, C.H., DeLand, M.T., Labow, G.J., Fleming, E.L., Weisenstein, D.K., Ko, M.K.W., Sinnhuber, M., Russell, J.M., 2005. Neutral atmospheric influences of the solar proton events in October–November 2003. J. Geophys. Res. Space Phys. 110 (A9), http://dx.doi.org/10.1029/2004JA010888.

Jackman, C.H., Randall, C.E., Harvey, V.L., Wang, S., Fleming, E.L., López-Puertas, M., Funke, B., Bernath, P.F., 2014. Middle atmospheric changes caused by the January and March 2012 solar proton events. Atmos. Chem. Phys. 14 (2), 1025–1038. http://dx.doi.org/10.5194/acp-14-1025-2014, URL https://acp.copernicus.org/articles/14/1025/2014/.

Kiviranta, J., Pérot, K., Eriksson, P., Murtagh, D., 2018. An empirical model of nitric oxide in the upper mesosphere and lower thermosphere based on 12 years of Odin SMR measurements. Atmos. Chem. Phys. 18 (18), 13393–13410. http://dx.doi.org/10.5194/acp-18-13393-2018, URL https://acp.copernicus.org/articles/18/13393/2018/.

Matzka, J., Bronkalla, O., Tornow, K., Elger, K., Stolle, C., 2021a. Geomagnetic kp index. v. 1.0. GFZ data services. http://dx.doi.org/10.5880/Kp.0001.

Matzka, J., Stolle, C., Yamazaki, Y., Bronkalla, O., Morschhauser, A., 2021b. The geomagnetic kp index and derived indices of geomagnetic activity. Space Weather 19 (5), http://dx.doi.org/10.1029/2020SW002641, e2020SW002641. URL arXiv:https://agupubs.onlinelibrary.wiley.com/doi/pdf/10.1029/2020SW002641.

McElroy, M.B., McConnell, J.C., 1971. Nitrous oxide: A natural source of stratospheric NO. J. Atmos. Sci. 28 (6), 1095–1098. http://dx.doi.org/10.1175/1520-0469(1971)028<1095:NOANSO>2.0.CO;2, URL https://journals.ametsoc.org/view/journals/atsc/28/6/1520-0469_1971_028_1095_noanso_2_0_co_2.xml.

Mironova, I., Aplin, K., Arnold, F., Bazilevskaya, G., Harrison, R., Krivolutsky, A., Nicoll, K., Rozanov, E., Turunen, E., Usoskin, I., 2015. Energetic particle influence on the earth's atmosphere. Space Sci. Rev. 194, http://dx.doi.org/10.1007/s11214-015-0185-4.

Nash, E., Newman, P., Rosenfield, J., Schoeberl, M., 1996. An objective determination of the polar vortex using Ertel's potential vorticity. J. Geophys. Res. 101, 9471–9478. http://dx.doi.org/10.1029/96JD00066.

Newnham, D.A., Clilverd, M.A., Rodger, C.J., Hendrickx, K., Megner, L., Kavanagh, A.J., Seppälä, A., Verronen, P.T., Andersson, M.E., Marsh, D.R., Kovács, T., Feng, W., Plane, J.M.C., 2018. Observations and modeling of increased nitric oxide in the antarctic polar middle atmosphere associated with geomagnetic storm-driven energetic electron precipitation. J. Geophys. Res. Space Phys. 123 (7), 6009–6025. http://dx.doi.org/10.1029/2018JA025507, URL arXiv:https://agupubs.onlinelibrary.wiley.com/doi/pdf/10.1029/2018JA025507.

Pérot, K., Orsolini, Y.J., 2021. Impact of the major SSWs of February 2018 and January 2019 on the middle atmospheric nitric oxide abundance. J. Atmos. Sol.-Terr. Phys. 218, 105586. http://dx.doi.org/10.1016/j.jastp.2021.105586.

Randall, C.E., Harvey, V.L., Singleton, C.S., Bailey, S.M., Bernath, P.F., Codrescu, M., Nakajima, H., Russell III, J.M., 2007. Energetic particle precipitation effects on the Southern Hemisphere stratosphere in 1992–2005. J. Geophys. Res.: Atmos. 112 (D8), http://dx.doi.org/10.1029/2006JD007696, arXiv:https://agupubs.onlinelibrary.wiley.com/doi/pdf/10.1029/2006JD007696.

Randall, C.E., Harvey, V.L., Siskind, D.E., France, J., Bernath, P.F., Boone, C.D., Walker, K.A., 2009. NOx descent in the Arctic middle atmosphere in early 2009. Geophys. Res. Lett. 36 (18), http://dx.doi.org/10.1029/2009GL039706, URL arXiv:https://agupubs.onlinelibrary.wiley.com/doi/pdf/10.1029/2009GL039706.

Rienecker, M.M., Suarez, M.J., Gelaro, R., Todling, R., Bacmeister, J., Liu, E., Bosilovich, M.G., Schubert, S.D., Takacs, L., Kim, G.-K., Bloom, S., Chen, J., Collins, D., Conaty, A., da Silva, A., Gu, W., Joiner, J., Koster, R.D., Lucchesi, R., Molod, A., Owens, T., Pawson, S., Pegion, P., Redder, C.R., Reichle, R., Robertson, F.R., Ruddick, A.G., Sienkiewicz, M., Woollen, J., 2011. MERRA: NASA's

modern-era retrospective analysis for research and applications. J. Clim. 24 (14), 3624–3648. http://dx.doi.org/10.1175/JCLI-D-11-00015.1, URL https://journals.ametsoc.org/view/journals/clim/24/14/jcli-d-11-00015.1.xml.

Rodgers, C., 2000. INverse Methods for Atmospheric Sounding: theory and Practise, first ed World Scientific Publishing.

Sagi, K., Murtagh, D., Urban, J., Sagawa, H., Kasai, Y., 2014. The use of SMILES data to study ozone loss in the Arctic winter 2009/2010 and comparison with Odin/SMR data using assimilation techniques. Atmos. Chem. Phys. 14 (23), 12855–12869. http://dx.doi.org/10.5194/acp-14-12855-2014, URL https://acp.copernicus.org/articles/14/12855/2014/.

Sinnhuber, M., Berger, U., Funke, B., Nieder, H., Reddmann, T., Stiller, G., Versick, S., von Clarmann, T., Wissing, J.M., 2018. NO_y production, ozone loss and changes in net radiative heating due to energetic particle precipitation in 2002–2010. Atmos. Chem. Phys. 18 (2), 1115–1147. http://dx.doi.org/10.5194/acp-18-1115-2018, URL https://acp.copernicus.org/articles/18/1115/2018/.

Sinnhuber, M., Friederich, F., Bender, S., Burrows, J.P., 2016. The response of mesospheric NO to geomagnetic forcing in 2002–2012 as seen by SCIAMACHY. J. Geophys. Res. Space Phys. 121 (4), 3603–3620. http://dx.doi.org/10.1002/2015JA022284, URL arXiv:https://agupubs.onlinelibrary.wiley.com/doi/pdf/10.1002/2015JA022284.

Sinnhuber, M., Nieder, H., Wieters, N., 2012. Energetic particle precipitation and the chemistry of the mesosphere/lower thermosphere. Surv. Geophys. 33 (6), 1281–1334. http://dx.doi.org/10.1007/s10712-012-9201-3.

Siskind, D.E., Barth, C.A., Russell III, J.M., 1998. A climatology of nitric oxide in the mesosphere and thermosphere. Adv. Space Res. 21 (10), 1353–1362. http://dx.doi.org/10.1016/S0273-1177(97)00743-6.

Siskind, D.E., Eckermann, S.D., Coy, L., McCormack, J.P., Randall, C.E., 2007. On recent interannual variability of the Arctic winter mesosphere: Implications for tracer descent. Geophys. Res. Lett. 34 (9), http://dx.doi.org/10.1029/2007GL029293, URL arXiv:https://agupubs.onlinelibrary.wiley.com/doi/pdf/10.1029/2007GL029293.

Taylor, J., 1982. An Introduction to Error Analysis: The Study of Uncertainties in Physical Measurements, second ed University Science Books, USA.

von Clarmann, T., Funke, B., López-Puertas, M., Kellmann, S., Linden, A., Stiller, G.P., Jackman, C.H., Harvey, V.L., 2013. The solar proton events in 2012 as observed by MIPAS. Geophys. Res. Lett. 40 (10), 2339–2343. http://dx.doi.org/10.1002/grl.50119, URL arXiv:https://agupubs.onlinelibrary.wiley.com/doi/pdf/10.1002/grl.50119.